Processes of DNA condensation induced by multivalent cations: Approximate annealing experiments and molecular dynamics simulations*

Chai Ai-Hua(柴爱华)[a)b)], Ran Shi-Yong(冉诗勇)[c)], Zhang Dong(张 冬)[a)], Jiang Yang-Wei(蒋杨伟)[a)], Yang Guang-Can(杨光参)[c)], and Zhang Lin-Xi(章林溪)[a)†]

[a)] *Department of Physics, Zhejiang University, Hangzhou* 310027, *China*
[b)] *College of Mathematics, Physics and Information Engineering, Jiaxing University, Jiaxing* 314001, *China*
[c)] *Department of Physics, Wenzhou University, Wenzhou* 325027, *China*

(Received 22 December 2012; revised manuscript received 15 March 2013)

The condensation of DNA induced by spermine is studied by atomic force microscopy (AFM) and molecular dynamics (MD) simulation in this paper. In our experiments, an equivalent amount of multivalent cations is added to the DNA solutions in different numbers of steps, and we find that the process of DNA condensation strongly depends on the speed of adding cations. That is, the slower the spermine cations are added, the slower the DNA aggregates. The MD and steered molecular dynamics (SMD) simulation results agree well with the experimental results, and the simulation data also show that the more steps of adding multivalent cations there are, the more compact the condensed DNA structure will be. This investigation can help us to control DNA condensation and understand the complicated structures of DNA–cation complexes.

Keywords: DNA condensation, multivalent cations, molecular dynamics simulation

PACS: 87.15.–v, 36.20.–r, 82.20.Wt **DOI:** 10.1088/1674-1056/22/9/098701

1. Introduction

It is well known that living cells naturally master the task of condensing and de-condensing DNA at specific times, such as in cell life cycles making the genetic code available for gene expression,[1,2] as well as in storing the long DNA structure into a compartment with dimensions on the order of microns.[3] In the gene replication and delivery process, such condensation is an important mechanism for protecting the genetic information from external factors. The details of the mechanism of DNA condensation are greatly helpful to us in understanding how the DNA is organized into chromatin, as well as in the development of gene delivery vehicles.[4,5]

DNA condensation, a fundamental process of life, has been the object of many investigations for a long time.[6,7] In fact, many agents can cause DNA molecules to collapse into more compact structures, such as alcohols,[8,9] neutral crowding polymers,[10–13] histone,[14,15] basic proteins,[16] multivalent cations,[3,17,18] cationic polypeptides,[19] and even positively charged surfaces.[20,21] It is worth noting that the DNA condensation induced by multivalent cations is particularly interesting because the process has many features in common with DNA packaged *in vivo*.[22] This DNA condensation depends primarily on the valence of the cations, rather than the cations' structure.[23] For example, a columnar hexagonal liquid crystalline packaging of DNA has been observed in the presence of polyamines and other multivalent cations.[24] At a critical extent of charge neutralization, the cations cause localized bending or distortion of DNA which facilitates the formation of rods and toroid-like structures.[25,26] Ran *et al.* investigated the morphology of the DNA-dodecyltrimethylammonium bromide (DTAB) complex,[27] and they found that the condensation behavior of DNA depends on the DTAB concentration and incubation time.

DNA condensation is a very complex process associated with many experimental conditions, such as the concentration of multivalent cations and the experimental temperature. This paper focuses on the DNA condensation induced by multivalent cations under various experimental protocols. In previous experiments, all of the cation solution was added to the DNA solution at once. However, in our experiments, an annealing concept is adopted to study the condensation process of the DNA–spermine complex. This means that all the DNA samples will receive the same amount of cations in the end but the cations will be added to the DNA samples in steps, with the number of steps differing for each sample. For clarity, a schematic illustration of adding cations in differing steps is shown in Fig. 1. In our experiments, spermine, one of the naturally occurring polyamines, is used to study the DNA condensation, and some interesting intermediate morphologies of the DNA condensation in different samples are observed by atomic force microscopy (AFM) imaging. The results show

*Project supported by the National Natural Science Foundation of China (Grant Nos. 20974081, 20934004, 21174131, and 21104060) and the Zhejiang Provincial Natural Science Foundation of China (Grant No. Y4110357).

†Corresponding author. E-mail: lxzhang@zju.edu.cn

© 2013 Chinese Physical Society and IOP Publishing Ltd

that the process of DNA condensation and the compactness of the condensates depend on the number of steps of adding spermine and the incubation time. In addition, a coarse-grained molecular dynamics (MD) model of DNA condensation has been developed and executed. The simulation results show that in a state of non-equilibrium the DNA condensations become more and more compact as cations are added in more and smaller steps, which agrees well with our experimental results. And the steered molecular dynamics (SMD) method is employed to detect the structures of the condensates. More details of the model and the simulation technique will be given in the following section.

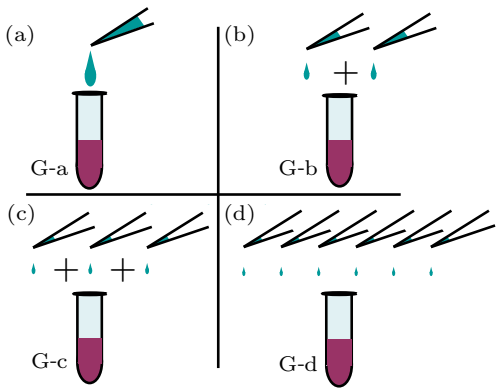


Fig. 1. Schematic diagram of approximate annealing experiments. The four samples are processed as follows: (a) adding spermine only once; (b) adding spermine twice; (c) adding spermine three times; (d) adding spermine six times.

2. Experimental and computational methods

2.1. Materials

Bacterial λ-phage DNA (0.5 μg/μL, 48500 bp) was purchased from New England Biolabs and used without further purification. The DNA solution was diluted to 1 ng/μL with $1 \times$ TE buffer containing 5 mM $MgCl_2$. Spermine (Nacalai Tesque, Japan) was dissolved to 100 μM for reserve. Water was deionized and purified by using a millipore system and had a conductivity less than 1×10^{-6} $\Omega^{-1}\cdot cm^{-1}$. Mica was cut into approximately 1 cm^2 square pieces and mica surfaces were always freshly cleaved before use.

2.2. Experimental methods

The approximate annealing experiments were performed following four protocols as follows.

Protocol 1) for sample G-a: 30 μL 100 μM spermine solution was added to 200 μL λ-DNA solution all at once, as shown in Fig. 1(a). This can be regarded as a rapid annealing. Here, we define the annealing speed to be inversely proportional to the occurrence of adding spermine. Namely, the more steps of adding cations, the slower the annealing speed.

Protocol 2) for sample G-b: 30 μL spermine was added to 200 μL λ-DNA solution in two steps. That is, only 15 μL spermine was added to the DNA solution each time, as shown in Fig. 1(b). The interval between the two adding operations was 10 min. In this way, the energy fluctuation of the system is smaller, which indicates that the annealing speed is slower.

Protocol 3) for sample G-c: 30 μL spermine was added to 200 μL λ-DNA solution in three increments. Here, each time, only 10 μL spermine was added to the DNA solution, as shown in Fig. 1(c). The interval between two adjacent operations was again 10 min. Hence the annealing process is much slower.

Protocol 4) for sample G-d: 30 μL spermine was added to 200 μL λ-DNA solution in six steps, as shown in Fig. 1(d). The interval was 10 min with 5 μL spermine at each step, so the annealing process was very slow this way. Here we would like to emphasize that all four final solutions contain 200 μL λ-DNA and 30 μL spermine.

2.3. Sample preparation

The incubation time started from the last drop of spermine. Several microliters of the mixture were extracted for observation at a series of time to investigate the DNA condensation processes. The extracted liquid was deposited onto freshly cleaved mica and incubated for 3 min. Following the incubation, the mica surface was washed gently with 100 μL Milli-*Q* filtered water 5–6 times to remove the free and excess molecules, and then rapidly blown dry using a gentle stream of nitrogen gas. After drying, the samples were kept in desiccators, ready for AFM scanning. All the operations above were performed at room temperature. It is important to note that in AFM sample preparation, the deposition, washing, and drying processes on mica may influence the morphology characterization. That is, the AFM images show the digitally flattened morphologies of the DNA condensates with their original compacted structures.

2.4. Atomic force microscopy imaging

An SPM-9600 system (Shimadzu, Kyoto, Japan) equipped with a J-scanner was employed to scan the samples. Most of the samples were scanned at a size of 5 μm × 5 μm in the tapping mode at the ambient condition with a scan speed of $\sim$ 2 Hz. The images were derived from the original data and flattened to improve the contrast grade.

2.5. Simulation details

In this work, we employ the LAMMPS molecular dynamics package[28] to perform Langevin dynamics in the *NVT* ensemble to study the dynamic behavior of DNA condensation induced by multivalent cations. The Coulomb interactions are handled by the particle-particle particle-mesh (PPPM) method.[29–31] The simulation includes two main processes. First, the initial DNA chains are positioned in a periodic box ($100\sigma \times 100\sigma \times 100\sigma$) randomly, which means that the initial positions of the DNA chains are random. The temperature is set to $T = 1.2$, the time step is $\tau = 0.001\tau_0$, where

$\tau_0 = (m\sigma^2/\varepsilon)^{1/2}$ (m is the mass of the monomer). Each simulation runs for minimum of 1×10^7 steps for the sake of equilibrium. Second, a certain amount of multivalent cations are added to the equilibrium DNA system in different numbers of stages, following the same patterns as in the experiment. Therefore, four different simulations are performed: 1) adding all at once; 2) adding in two steps; 3) adding in three times; 4) adding in six times. In the simulation, the interval of any two adjacent adding cations is set to be 1×10^5 simulation steps and the total quantities of multivalent cations in every simulation are the same. Additionally, we restart the simulations after all cations have been added to the DNA system and all the measures mentioned below are carried out after this point. The above simulation method is highly comparable to an annealing algorithm, so it is called the approximate annealing algorithm simulation.

In the simulations, a coarse-grained model of DNA condensation induced by multivalent cations under good solvent conditions is investigated. We model the DNA chains by employing the Kratky–Porod worm-like chain,[32,33] which is widely used in the polymer chain simulations.[34,35] In the coarse-grained model, a DNA chain contains $N = 200$ monomers and is charged negatively. The potential of the DNA chain is

$$U_c = 4\varepsilon\left[\left(\frac{\sigma_{ij}}{r_{ij}}\right)^{12} - \left(\frac{\sigma_{ij}}{r_{ij}}\right)^{6} + \frac{1}{4}\right] - \frac{1}{2}K\left(\frac{l_0}{\sigma}\right)^2 \ln\left[1 - \left(\frac{r_{ij}}{l_0}\right)^2\right] + K_b(1 + \cos\Phi), \quad (1)$$

where the first term is the Lennard–Jones potential with a cut distance $2^{1/6}\sigma$ between any two monomers, the second term is an FENE spring with a cut distance l_0 between the neighboring monomers, and the last term is an angle potential which describes the bending rigidity of the DNA chain. Here r_{ij} is the distance between the centers of monomers i and j, Φ is the angle between two adjacent bond vectors, and $\sigma_{ij} = \sigma = 1$, $\varepsilon = 1.0k_BT$, $K = 30k_BT$, $l_0 = 1.5\sigma$, $K_b = 10k_BT$.

Spermine is a relatively narrow molecule, which can approach DNA at close proximity, and even penetrate the grooves at certain sites and orientations.[36] Therefore, the multivalent cations can be treated as a kind of positively charged short polymer chain (PCSPC). In our simulation, each PCSPC contains 5 monomers with monomer diameter $\sigma' = \sigma$, and both ends of the PCSPC are +4 positively charged. That is, the three intermediate monomers of the PCSPC are neutral. The potential of the PCSPC can also be described by Eq. (1) with $\varepsilon' \to \varepsilon$, $\sigma' \to \sigma$, $K' \to K$, $l_0' \to l_0$, $b \to K_b$, and $\theta \to \Phi$. The parameters are chosen to be $\varepsilon' = 1.0k_BT$, $K' = 30k_BT$, $l_0' = 1.5\sigma'$, and $b = 200k_BT$.

In the present model, all charged particles in the system interact via the electrostatic Coulombic potential

$$U_{el}(r_{ij}) = \frac{q_i q_j}{4\pi\varepsilon_0\varepsilon_r r_{ij}}, \quad (2)$$

where ε_0 is the dielectric constant with the relative dielectric constant $\varepsilon_r = 1.0$, q_i and q_j are the charges on the two monomers.

At last, steered molecular dynamics (SMD)[37,38] is employed to investigate the unzipping process of the compact DNA chains. A Hookean spring with force constant $k_0 = k_BT/\sigma^2$ is attached at one end of the DNA chain, and it moves with a constant velocity $v_0 = \sigma/\tau$ in the x-axis direction. The force acting on the end of the DNA chain is recorded at every time step, i.e., $f(t) = k_0 \times (x(0) - x(t))$,[37] where $x(t)$ is the displacements between one of the end monomers and the spring's end point, and $x(0)$ is the equilibrium value of the spring length.

3. Results and discussion

3.1. Experimental formations of DNA condensation

We conducted the experiments following four different protocols and using four identical samples. The AFM images of the DNA–spermine complex morphologies are exhibited in Fig. 2 for different incubation times (horizontal) and in different experimental samples (vertical). The results with rapidly annealed process are shown in the first row in Fig. 2. Figure 2(a-1) shows that the DNA chains begin to fold immediately after spermine is adding to the solution. Nevertheless, the distributions of the DNA chains are still homogeneous. When the incubation time equals 5 min, the DNA chains fold into small dishes in local structures as shown in Fig. 2(a-2). After a longer incubation time, about 10 min, the DNA chains collapse into rod/star structures (see Fig. 2(a-3)). This indicates that the condensation degree is further strengthened. After 60 min ($t = 60$ min), all the DNA chains have been compacted into globular structures (see Fig. 2(a-4)). Obviously, all the final morphologies of DNA chains are very compact globular structures, as shown in the last column. The difference is that each sample has its own initial condensed form. Furthermore, as shown in the first column in Fig. 2, the formation of the DNA in image (b-1) is more compact than that of the DNA in image (a-1). In image (c-1), a kind of mesh structure made up of irregular small clumps and bold chains is observed. In the last image (d-1) of the first column, it can be seen that the DNA chains have collapsed into irregular large clumps. This indicates that the condensation of the DNA becomes more and more compact as the number of steps of adding cations increases. Here, it should be noted that the incubation time mentioned before is only for the sampling time, and the depositing time is not included. Another interesting phenomenon is that, as the annealing speed slows down, the phase transition speed of the DNA becomes slower. Comparing the formations of DNA imaged from different samples, it seems that the condensation behavior of DNA depends on the annealing speed as well as the incubation time.

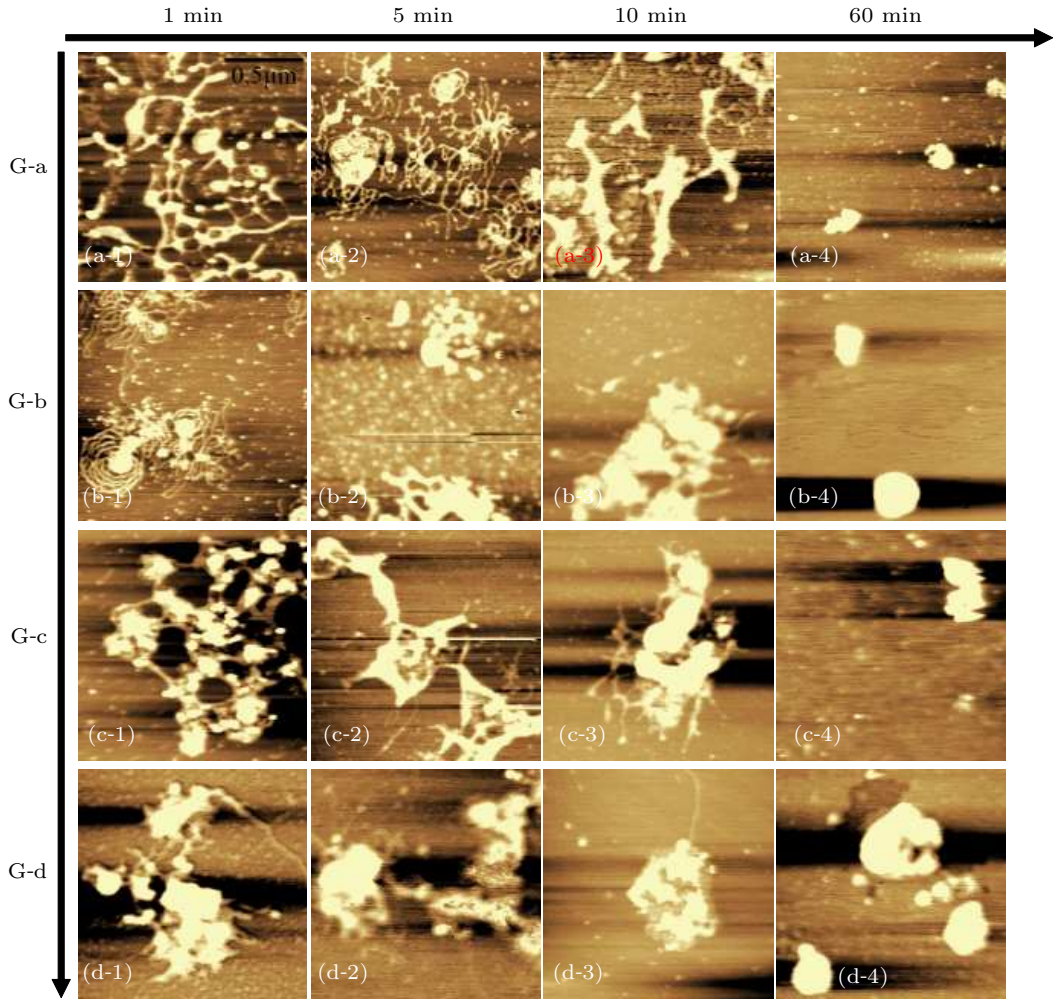


Fig. 2. (color online) Typical images of the DNA–spermine complexes with varying incubation time in different samples. From left to right, the incubation time is 1 min, 5 min, 10 min, and 60 min, respectively. From top to bottom, samples are (a) G-a, (b) G-b, (c) G-c, and (d) G-d, respectively.

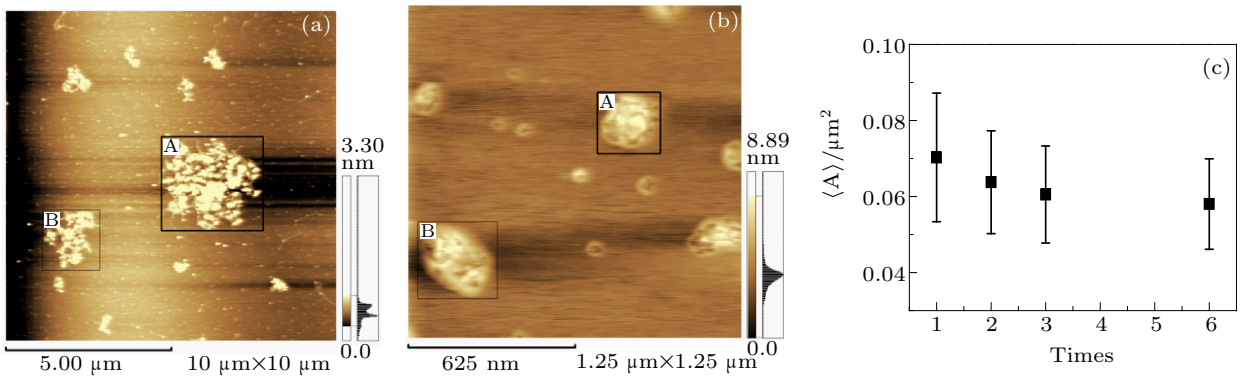


Fig. 3. (color online) Images of the morphology of DNA–spermine complexes induced by different doses of spermine. The DNA solution contains (a) 15 μL or (b) 30 μL spermine. (c) The average area $\langle A \rangle$ of condensed DNA measured by AFM offline analysis vs. number of steps of adding spermine.

We also investigate the effects of adding two different doses of spermine on the final morphologies of the DNA–spermine complex and the results are shown in Fig. 3. When the DNA solution contains only 15 μL spermine, the final morphology of the DNA–spermine complex is loose, as shown in Fig. 3(a). The sizes of those aggregates have been measured through AFM offline analysis. Interestingly, the results show that the sizes are not the same, the typical sizes are from 3.2 μm^2 (like block B in Fig. 3(a)) to 8.8 μm^2 (block A). Figure 3(b) shows the compact globular structures of the DNA when the solution contains 30 μL spermine. The average areas $\langle A \rangle$ of condensed DNA in different experimental samples

are plotted in Fig. 3(c), and the value decreases as the number of steps of adding spermine increases. The results show that the slower the spermine cations are added, the smaller the condensed DNA morphology is. Therefore, both the spermine concentration and the speed of adding spermine play an important role on the final condensed DNA structure.

3.2. Simulation process of DNA condensation

Four different condensation processes of the DNA–cation complex have been simulated using MD simulation and the typical formations are shown in Fig. 4. The first row shows the morphologies of the DNA chains for the simulation of the first sample. When $t = 1 \times 10^4 \tau$, the distribution of DNA chains is very homogeneous, as shown in Fig. 4(a-1). As the simulation time increases, the DNA chains fold into small patches (Fig. 4(a-2)), and then those tiny patches combine into clusters (Fig. 4(a-3)). After a long simulation time, about $5 \times 10^5 \tau$, all DNA chains collapse into compact irregular coils (Fig. 4(a-4)). In this process, the phase transitions of DNA chains lead to many intermediate states. As for other formations of the DNA chains, shown in Fig. 4, the results indicate that the more steps there are of adding PCSPCs, the fewer intermediate states of DNA condensation occur. For example, in the 4th row, while adding PCSPCs in six steps, the DNA chains collapse partly at the beginning of the simulation, as shown in Fig. 4(d-1). Subsequently, the condensation process of the DNA becomes incredibly slow. That is, as the simulation time increases from $1 \times 10^4 \tau$ to $5 \times 10^5 \tau$, the morphology of the DNA changes from small compact irregular coils (Fig. 4(d-1)) to highly compact irregular coils (Fig. 4(d-4)). We have to point out that the simulation has not reached equilibrium at $5 \times 10^5 \tau$. When $t > 5 \times 10^5 \tau$, the DNA condensates assume almost the same morphology in all simulations. In this paper, we focus on the different condensation processes of DNA chains undergoing different annealing speeds, therefore the simulation results after $t = 5 \times 10^5 \tau$ are ignored. In general, these characteristics of the DNA phase transition obtained from simulations agree well with the experiments.

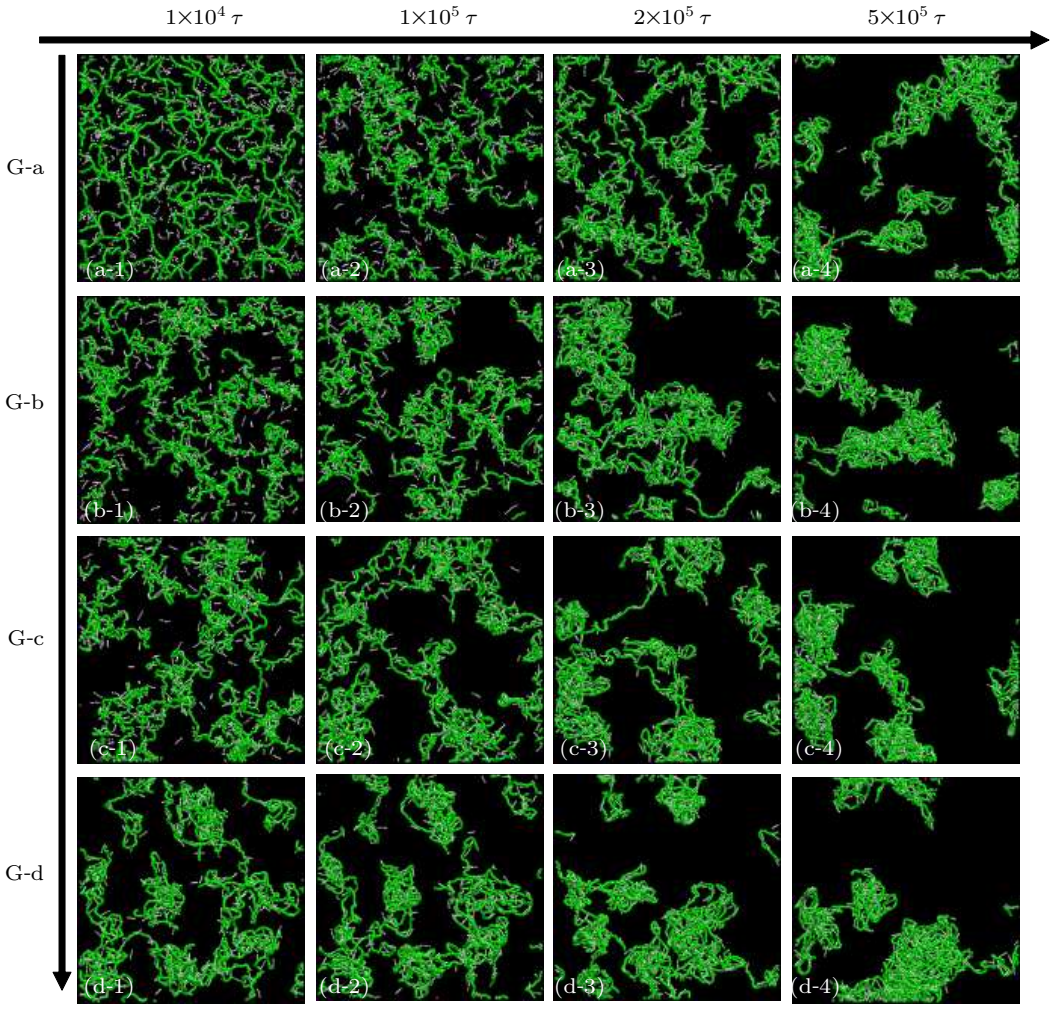


Fig. 4. (color online) Typical formations of DNA with varying simulation times, obtained from different MD simulations. From left to right, the simulation time is $1 \times 10^4 \tau$, $1 \times 10^5 \tau$, $2 \times 10^5 \tau$, and $5 \times 10^5 \tau$, respectively. From top to bottom, simulations are for samples (a) G-a, (b) G-b, (c) G-c, and (d) G-d, respectively.

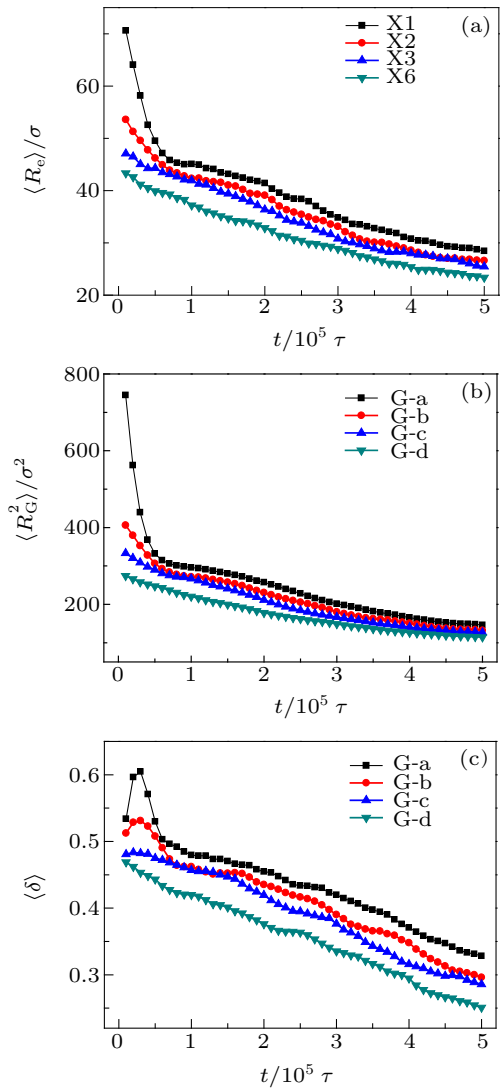


Fig. 5. (color online) (a) Mean end-to-end distance $\langle R_e \rangle$, (b) mean-square radius of gyration $\langle R_G^2 \rangle$, and (c) shape factor $\langle \delta \rangle$ of the DNA chains as a function of the simulation time t for each simulation.

To obtain the details of the DNA condensation, we calculate the mean end-to-end distance $\langle R_e \rangle$ and the mean-square radius of gyration $\langle R_G^2 \rangle$ to describe the average size of the DNA chains, as well as the shape factor $\langle \delta \rangle$ to describe the shape of the DNA chains. These parameters were used well in previous research to explain the formation behavior of the polymers.[39,40] In Fig. 5(a), we plot $\langle R_e \rangle$ as a function of the simulation time t. For once adding positively charged short polymer chains to the DNA system, there is a sharp decrease of $\langle R_e \rangle$ at the beginning of the simulation $t < 7 \times 10^4 \tau$, this indicates that the DNA chains collapse very quickly. As the simulation continues, the slope of the curve becomes small, it implies that the collapse is slowing down. For adding PCSPCs twice, a quick decrease also appears at the beginning of the simulation, however, it is not precipitous like the previous one. In the cases of adding PCSPCs three times and six times, the decreases become slow in the curves. On the whole, when $t > 8 \times 10^4 \tau$, all the curves in Fig. 5(a) decrease smoothly. This implies that during this time all the DNA chains in different simulations collapse stably. This condensation characteristic of DNA is also confirmed by the curves of $\langle R_G^2 \rangle$ in Fig. 5(b). Moreover, all $\langle R_G^2 \rangle$ trend to the same value. This indicates that the aggregates are almost of the same size. The results agree well with the experiments. As plotted in Fig. 5(c), all the values of shape factor $\langle \delta \rangle$ decrease smoothly and monotonously except for a fluctuation for simulation a or b in the prior simulation period. In addition, it is found that the values of the curves decrease as the number of steps of adding PCSPCs increases. Namely, the slower the annealing, the more compact the condensed DNA structure. This characteristic can help us to control the condensation process of the DNA well.

In order to obtain more information about the compact structure of DNA condensation, we calculate the average spacing of adjacent nodes $\langle L \rangle$ and the average density of nodes per DNA chain $\langle \rho \rangle$, where L is the spacing between any two adjacent nodes on one chain as the insert shown, and ρ is the density of nodes, i. e., $\rho = N_{\text{node}}/N$. Here N_{node} represents the number of nodes, and N is the number of monomers in a DNA chain. The inset in Fig. 6(a-1) is a schematic diagram of the nodes that are the combination points of DNA chains and PCSPCs. We analyze the formation properties of DNA chains at three moments: $t = 1 \times 10^4 \tau$, $1 \times 10^5 \tau$, and $2 \times 10^5 \tau$, and the results are shown in Fig. 6. In Fig. 6(a-1) with $t = 1 \times 10^4 \tau$, the values of $\langle L \rangle$ are very large (about 27σ in the case of adding PCSPCs only once), and it decreases to $\langle L \rangle = 10\sigma$ for the case of twice adding. As the steps of adding PCSPCs increase, $\langle L \rangle$ decreases, as shown in Fig. 6(a-1). The red curve shows a completely different trend. That is, in the case of adding all at once, the mean density of nodes $\langle \rho \rangle$ is very low, meaning that there are few nodes on the DNA chains. Therefore, the condensation degree of DNA is low. When the steps of adding increase to six, the value of $\langle \rho \rangle$ approaches 0.2, and the condensation degree is higher in this case. Furthermore, to quantify the characteristics of the DNA condensation, the probability distribution P of different spacing of adjacent nodes is employed and is shown in Fig. 6. Figure 6(a-2) gives the values of P for the four different simulations at $t = 1 \times 10^4 \tau$. From the first row, we find that the value of L varies from as small as $L = 2\sigma$ to as large as $L = 180\sigma$, and a large value of L, such as $L > 100\sigma$, indicates that the DNA chains are very loose. Therefore, there are a few nodes on a DNA chain. This conclusion is consistent with the experimental results (Fig. 2(a-1)). In the second row, a very large L disappears and most of the values of L are smaller than 100. When the steps of adding increase to three (the 3rd row) and six (the 4th row), small values are most probable for L, as shown in Fig. 6(a-2). The small values of L indicate that the condensation degree of DNA becomes higher. When the simulation time increases to $1 \times 10^5 \tau$ and $2 \times 10^5 \tau$, the results are shown in Figs. 6(b-1), 6(b-2) and 6(c-1), 6(c-2), respectively. From those figures, it can be seen that with an increase in the number of adding steps, $\langle L \rangle$ decreases and $\langle \rho \rangle$ increases; meanwhile, the distribution of P moves toward the small L (2σ–5σ). This indicates that the condensation degree of DNA becomes higher, and that the condensation process of DNA is really related with the number of steps of adding PCSPCs.

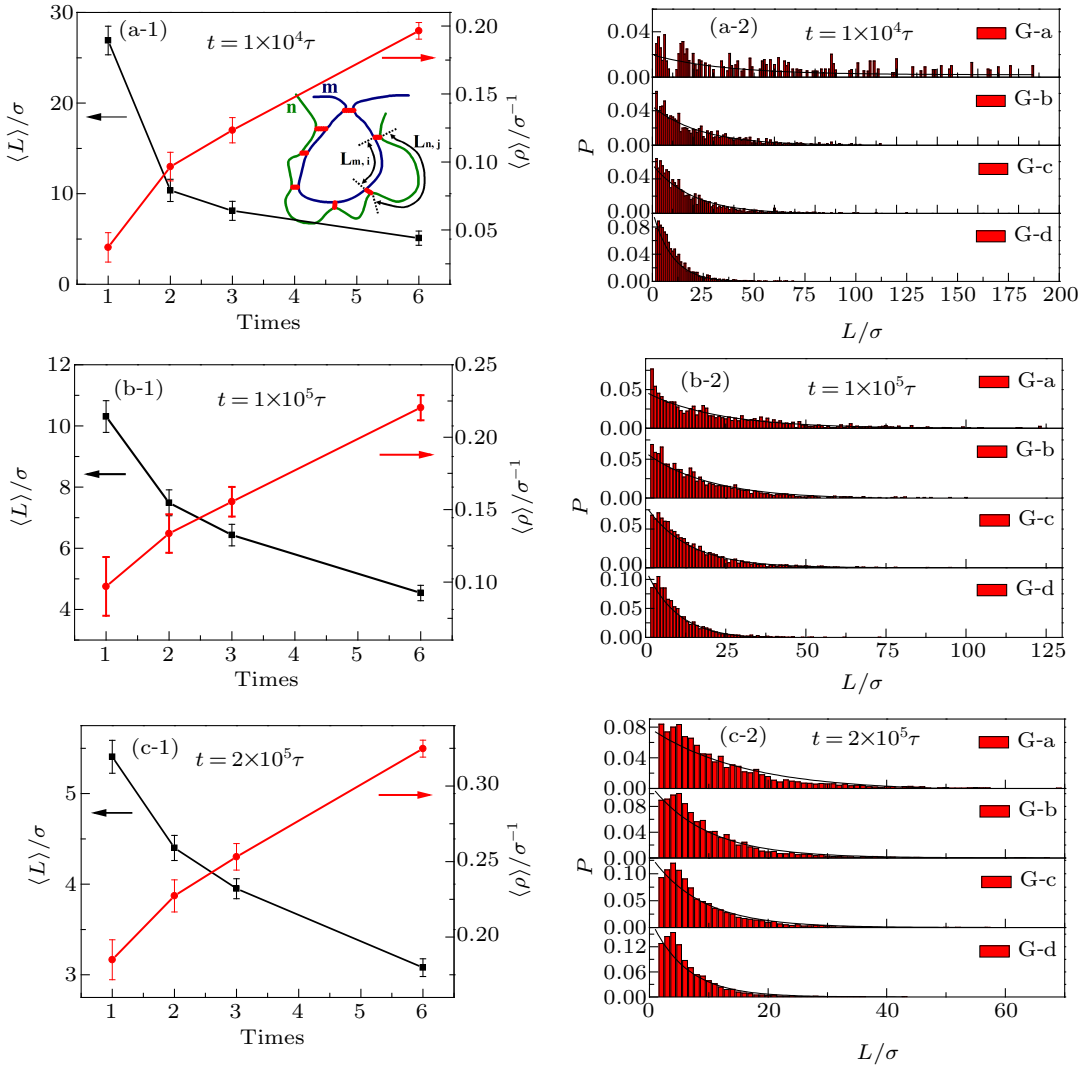


Fig. 6. (color online) Average spacing of adjacent nodes $\langle L\rangle$ and average density of nodes per DNA chain $\langle\rho\rangle$ as a function of time of adding positively charged short polymer chains at different simulation time: (a-1) $t = 1\times10^4\tau$, (b-1) $1\times10^5\tau$, and (c-1) $2\times10^5\tau$. Insert shows a schematic diagram of the nodes which are the combination points of DNA chains and PCSPCs. Probability distribution P of different spacing of adjacent nodes as a function of L at different simulation time: (a-2) $t = 1\times10^4\tau$, (b-2) $1\times10^5\tau$, and (c-2) $2\times10^5\tau$.

3.3. Steered molecular dynamics study of the DNA structure

Condensation structures of DNA depend on the number of steps of adding PCSPCs as well as the multivalent cation concentration. In order to understand the mechanical properties of compact DNA chains, we employ steered molecular dynamics (SMD) to explore the internal formation of the collapsed DNA chains at the moment of $t = 1\times10^5\tau$. It must be emphasized that the formations, which have been unzipped by means of SMD, are in non-equilibrium states. Figure 7(a) gives a schematic illustration of the steered molecular dynamics of the unzipping process with a harmonic spring of stiffness K_0 at a constant velocity v_0. In SMD, time-dependent external forces are applied to the DNA–cation system, and the responses of the system are analyzed by recording the positions of the harmonic spring. Figure 7(b) shows the external force exerted on the DNA chains $f(t)$ as a function of simulation time t with a constant velocity $v_0 = \sigma/\tau$. In the case of adding PCSPCs just once (Fig. 7(b-1)), most peaks in the curve are single-peaks; for clarity, we mark symbol ⊓ on the curve. The rapid decline following the single peak implies that the adjacent nodes spacing L is long and the formation of DNA chains is loose, as the schematic diagram shown under the curve. Figure 7(b-2) plots the force curve in the case of adding PCSPCs twice. Besides the single peak, there are several multi-peaks on this curve, marked by symbol O. The multi-peaks mean that L is shorter and the degree of DNA condensation becomes higher as the inset shows. When the steps of adding PCSPCs increase, there are many more multi-peaks in the curve as shown in Figs. 7(b-3) and 7(b-4). Therefore, the average adjacent nodes spacing $\langle L\rangle$ becomes much shorter and the DNA becomes more compact. This exactly proves that with more steps of adding PCSPCs the condensed DNA structure becomes more compact.

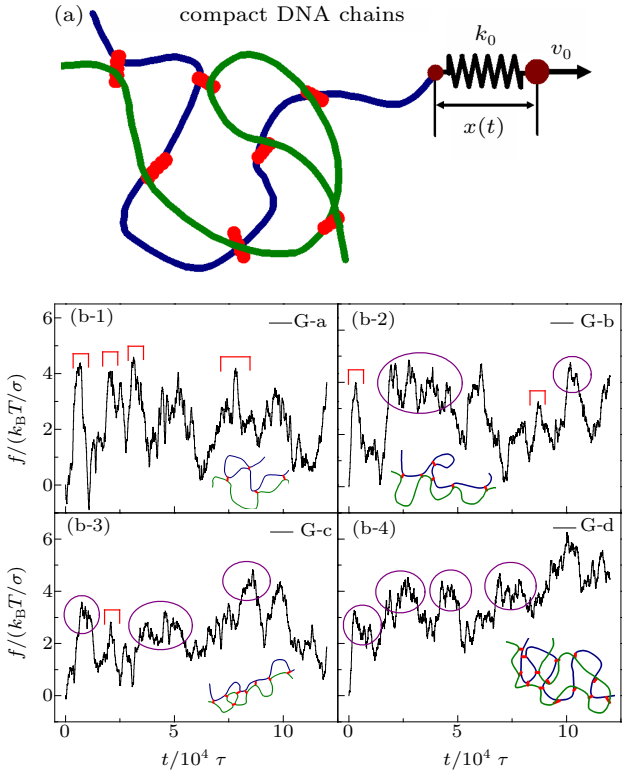


Fig. 7. (color online) (a) Schematic illustration of the steered molecular dynamics of the unzipping process with a harmonic spring of stiffness k_0 at a constant velocity v_0. (b) Force applied to one end of the compact DNA chains along the pulling direction during the process of unzipping the compact DNA chains adding positively charged short polymer chains in different numbers of steps: (b-1) one time, (b-2) two times, (b-3) three times, and (b-4) six times. The unzipping process begins at the simulation time $t = 1 \times 10^5 \tau$ after all PCSPCs are added to the DNA system.

3.4. Conclusions

Experimentally, we have used AFM to investigate the DNA condensation induced by spermine in different experimental protocols. The condensation behaviors of DNA depend on the protocol of adding multivalent cations, which is considered to be analogous to varying the annealing speed. In the case of very quick annealing, the DNA chains condense quickly to the compact globular final formation, and many intermediate phases are observed during the condensation process. In contrast, while adding cations in six steps, the DNA phase transition is very slow. This means that, in the case of relatively slow annealing, the energy fluctuation of the DNA–spermine solution is relatively weak and controlling the process of DNA condensation becomes relatively easy correspondingly.

In our simulations, the MD method has been employed to investigate the condensation of DNA induced by multivalent cations, and the results agree well with the experiments. This means that adding PCSPCs in more stages will help to minimize the energy fluctuation in the DNA–spermine system. Furthermore, in the case of non-equilibrium states, we find that the slower the PCSPCs are added, the more compact the condensed DNA structure is. In addition, the steered MD is used to stretch out the condensed DNA, and the force-extension curves also indicate that the compactness of the DNA condensation depends on the times of adding PCSPCs. This investigation can help us to understand the complicated structures of DNA–cation complexes.

References

[1] Jenuwein T and Allis C D 2001 *Science* **293** 1074
[2] Bednar J, Horowitz R A, Grigoryev S A, Carruthers L M, Hansen J C, Koster A J and Woodcock C L 1998 *Proc. Natl. Acad. Sci. USA* **95** 14173
[3] Bloomfield V A 1996 *Curr. Opin. Struct. Biol.* **6** 334
[4] Blessing T, Remy J S and Behr J P 1998 *Proc. Natl. Acad. Sci. USA* **95** 1427
[5] Montigny W J, Houchens C R, Illenye S, Gilbert J, Coonrod E, Chang Y C and Heintz N H 2001 *Nucleic Acids Res.* **29** 1982
[6] Ritort F, Mihardja S, Smith S B and Bustamante C 2006 *Phys. Rev. Lett.* **96** 118301
[7] Zinchenko A A, Yoshikawa K and Baigl D 2005 *Phys. Rev. Lett.* **95** 228101
[8] Wang Y W, Ran S Y, Man B Y and Yang G C 2011 *Soft Matter* **7** 4425
[9] Kleideiter G and Nordmeier E 1999 *Polymer* **40** 4013
[10] Lerman L S 1971 *Proc. Natl. Acad. Sci. USA* **68** 1886
[11] Vasilevskaya V V, Khokhlov A R, Matsuzawa Y and Yoshikawa K 1995 *J. Chem. Phys.* **102** 6595
[12] Zhang D, Chai A H, Wen X H, He L L, Zhang L X and Liang H J 2012 *Soft Matter* **8** 2152
[13] Dai F Y, Wang P F, Wang Y, Tang L, Yang J H, Liu W G, Li H X and Wang G C 2008 *Polymer* **49** 5322
[14] Li W, Wang P Y, Dou S X and Tong P Q 2003 *Chin. Phys.* **12** 226
[15] Ran S Y, Wang X L, Fu W B, Lai Z H, Wang W C, Liu X Q, Mai Z H and Li M 2006 *Chin. Phys. Lett.* **23** 504
[16] Kundu T K and Rao M R S 1995 *Biochemistry* **34** 5143
[17] Schnurr B, MacKintosh F C and Williams D R M 2000 *Europhys. Lett.* **51** 279
[18] Ou Z Y and Muthukumar M 2005 *J. Chem. Phys.* **123** 074905
[19] Bloomfield V A 1997 *Biopolymer* **44** 269
[20] Fang Y and Hoh J H 1998 *Nucleic Acids Res.* **26** 588
[21] Cao Q Q, Zuo C C, Ma Y H, Li L J and Zhang Z 2011 *Soft Matter* **7** 506
[22] Widom J and Baldwin R L 1980 *J. Mol. Biol.* **144** 431
[23] Widom J and Baldwin R L 1983 *Biopolymers* **22** 1595
[24] Saminathan M, Thomas T, Shirahata A, Pillai C K S and Thomas T J 2002 *Nucleic Acids Res.* **30** 3722
[25] Rouzina I and Bloomfield V A 1998 *Biophys. J.* **74** 3152
[26] Golan R, Pietrasanta L I, Hsieh W and Hansma H G 1999 *Biochemistry* **38** 14069
[27] Ran S Y, Wang Y W, Yang G C and Zhang L X 2011 *J. Phys. Chem. B* **115** 4568
[28] Plimpton S 1995 *J. Comp. Phys.* **117** 1
[29] Deserno M and Holm C 1998 *J. Chem. Phys.* **109** 7678
[30] Deserno M and Holm C 1998 *J. Chem. Phys.* **109** 7694
[31] Eastwood J W, Hockney R W and Lawrence D N 1980 *Comput. Phys. Commun.* **19** 215
[32] Porod G 1949 *Monatsh. Chem.* **80** 251
[33] Kratky O and Porod G 1949 *Recl. Trav. Chim. Pays-Bas.* **68** 1106
[34] Li D, Banon S and Biswal S L 2010 *Soft Matter* **6** 4197
[35] Koslover E F and Spakowitz A J 2009 *Phys. Rev. Lett.* **102** 178102
[36] Korolev N, Lyubartsev A P, Laaksonen A and Nordenskiöld L 2002 *Biophys. J.* **82** 2860
[37] Izrailev S, Stepaniants S, Balsera M, Oono Y and Schulten K 1997 *Biophys. J.* **72** 1568
[38] Kosztin D, Izrailev S and Schulten K 1999 *Biophys. J.* **76** 188
[39] Shen Y and Zhang L X 2005 *J. Polym. Sci. Part B Polym. Phys.* **43** 223
[40] Su J Y and Zhang L X 2007 *Polymer* **48** 7419